World Electric Vehicle Journal

MDPI

Article

Energy-Optimal Speed Control for Autonomous Electric Vehicles Up- and Downstream of a Signalized Intersection

Simin Hesami [1,*], Cedric De Cauwer [1], Evy Rombaut [2], Lieselot Vanhaverbeke [2] and Thierry Coosemans [1]

[1] The Mobility, Logistics, and Automotive Technology Research Center, Department of Electrical Engineering and Energy Technology, Vrije Universiteit Brussel, Laarbeeklaan 103, 1090 Brussels, Belgium
[2] The Mobility, Logistics, and Automotive Technology Research Center, Department of Business Technology and Operations, Vrije Universiteit Brussel, Laarbeeklaan 103, 1090 Brussels, Belgium
* Correspondence: simin.hesami@vub.be

Abstract: Signalized intersections can increase the vehicle stops and consequently increase the energy consumption by forcing stop-and-go dynamics on vehicles. Eco-driving with the help of connectivity is a solution that could avoid multiple stops and improve energy efficiency. In this paper, an eco-driving framework is developed, which finds the energy-efficient speed profile both up- and downstream of a signalized intersection in free-flow situations (eco-FF). The proposed framework utilizes the signal phasing and timing (SPaT) data that are communicated to the vehicle. The energy consumption model used in this framework is a combination of vehicle dynamics and time-dependent auxiliary consumption, which implicitly incorporates the travel time into the function and is validated with real-world test data. It is shown that, by using the proposed eco-FF framework, the vehicle's energy consumption is notably reduced.

Keywords: eco-driving; energy efficiency; real-world measurements

Citation: Hesami, S.; De Cauwer, C.; Rombaut, E.; Vanhaverbeke, L.; Coosemans, T. Energy-Optimal Speed Control for Autonomous Electric Vehicles Up- and Downstream of a Signalized Intersection. *World Electr. Veh. J.* **2023**, *14*, 55. https://doi.org/10.3390/wevj14020055

Academic Editors: Danial Karimi and Amin Hajizadeh

Received: 19 December 2022
Revised: 10 February 2023
Accepted: 15 February 2023
Published: 17 February 2023

1. Introduction

1.1. Context

In recent years, the transportation sector has been responsible for more than 28% of the total energy consumption and 26% of the greenhouse gas (GHG) emissions in the U.S. [1]. One-fourth of these emissions are caused by urban transportation delays at red traffic lights [2]. Signalized intersections are an important factor in energy consumption and GHG emissions, as well as the mobility hindrances because of the stop-and-go nature of traveling through a signalized arterial.

With the growth of intelligent transportation systems (ITS) and connected vehicle (CV) technology, a vehicle can obtain accurate information about the surrounding traffic conditions. Vehicle-to-infrastructure (V2I) and vehicle-to-vehicle (V2V) communication allow for the vehicle to access signal phasing and timing (SPaT) information, and learn the preceding vehicle's position, speed and acceleration [3–5].

These data can be used in the vehicle's motion planning in ecological driving (eco-driving) to improve the vehicle's behavior. Eco-driving comprises adjustments in driving behavior such as speed, acceleration rate, etc., in order to improve energy efficiency, mobility, emissions and/or congestion.

The goal of this paper is to develop an energy-optimal eco-driving system for a single automated electric vehicle (AEV) when the vehicle is approaching and departing from a traffic light using the V2I communication information.

1.2. Literature Review

There has been a large amount of research worldwide regarding energy efficiency improvements, looking at mobility, emission, safety, and congestion. At the early stages of energy economic control strategies, the cruising speed was optimized based on the vehicle's

internal characteristics [6] or road topography [7,8]. Other strategies adjusted the vehicle's speed or acceleration rate to reduce energy loss. Most studies focus on the eco-driving of a single vehicle, either in the vicinity of an isolated signalized intersection [9–12] or at an arterial of multiple intersections [13,14].

In [15], a fuel-efficient control strategy for a group of vehicles was developed, in which each vehicle was optimized separately in a decentralized manner. An ecological cooperative adaptive cruise control (CACC) for platoons was investigated in [5,16].

Some research works have prioritized traffic flow over energy efficiency and, in fact, can be considered speed/acceleration advisory systems by reducing the idling time at the red phase of the traffic light [17–19]. Other works jointly optimize a weighted sum of travel time and energy efficiency [20–22].

In the existing literature on driver assistance systems, speed advisory systems and eco-driving, most studies focus on the energy consumption formulation of internal combustion engines (ICE) such as the Virginia Tech Comprehensive Power-Based Fuel Consumption Model (VT-CPFM) [4,23,24] and VT-micro [9,11,25]. The formulation and solution of eco-driving control problems in EVs and internal combustion engine (ICE) vehicles are fundamentally different [26]. However, there are limited research works on the eco-driving of electric vehicles (EVs) [26–28] and, among those, the auxiliary consumption has mostly been ignored [26,28]. Other works minimize a weighted sum of the consumed energy and travel time [20–22]. To the best of the authors' knowledge, no paper has incorporated energy use and time-dependent auxiliary consumption in a single objective function.

When a vehicle leaves an intersection, it usually accelerates back to a desired set speed or the speed limit. The speed at which the vehicle reaches the intersection affects its energy consumption after it leaves the intersection. Therefore, optimizing a joint problem ,including up- and downstream, leads to better results rather than two separate problems. In the majority of the existing literature, the vehicle's departure behavior has not been investigated.

In this paper, the optimization problem was formulated with the objective of minimizing energy consumption. This consisted of the incorporation of vehicle dynamics and time-dependent auxiliary consumption. The proposed objective function minimizes the energy consumption, while not allowing for the travel time to have irrational values. This approach is much closer to a realistic energy modeling due to the consideration of an important cause of energy consumption, and does not require complicated weight-factor-tuning processes. Furthermore, the proposed eco-FF framework jointly controls and optimizes the approaching and departure behavior in free-flow situations. Normally, the decision/control variable of eco-driving problems is speed or acceleration. The travel time duration depends on the speed and acceleration rate. This makes the calculation of the energy consumption that is integrated over time impossible. Thus, we propose an analytical method that parameterizes the energy consumption as a function of speed and acceleration rate.

Therefore, the main contributions of this paper are as follows:

- Incorporating the vehicle dynamics and time-dependent auxiliary consumption as a single objective function that accurately models the real-world situation.
- Implementation of a joint eco-approach-and-departure strategy to achieve a global optimum.
- Analytical parameterization of vehicle's possible motion strategies to eliminate the time variable in the optimization.

In terms of the paper layout, first, the proposed joint model and its analytical parameterization process is presented in Section 2. Section 3 discusses the calibration and validation of the proposed energy consumption model, followed by the numerical results of the eco-FF framework. Finally, in Section 4, the conclusion and future work ideas are presented.

2. Materials and Methods

In this paper, we focus on the eco-driving of an AEV through an urban single-lane road while approaching and departing from a signalized intersection. The intersection is assumed to have a road side unit (RSU) that can broadcast the SPAT information to the vehicles via a dedicated short-range communication (DSRC). We assume that the vehicle enters the DSRC range with a known speed (v_i), and should reach the desired speed (v_d) when it arrives at a certain distance from the traffic light in the downstream.

2.1. Energy Consumption Modeling

The longitudinal vehicle dynamics based on Newton's second law of motion is

$$ma = F_w - \frac{1}{2}\rho C_a A_f v^2 - mg\mu cos(\theta) - mgsin(\theta), \tag{1}$$

where m is the vehicle's mass, a is the longitudinal acceleration of the vehicle, F_w is the sum of traction and braking force at the wheels, ρ is the air density, C_a is the aerodynamic drag coefficient, A_f is the frontal area of the vehicle, v is the longitudinal speed of the vehicle, g is the gravitational acceleration, μ is the friction coefficient, and θ is the road grade.

The instantaneous power ($P_w(t)$) needed at the wheels is

$$P_w(t) = F_w(t)v(t). \tag{2}$$

Therefore, the kinematic energy needed to travel through the road during $\Delta t = t_f - t_i$ unit of time is

$$E_w = \int_{t_i}^{t_f} F_w(t)v(t)dt = \frac{1}{\eta_D}\int_{t_i}^{t_f}(\eta_r ma(t)v(t) + \frac{1}{2}\rho CAv^3(t) + mg(\mu cos(\theta) + sin(\theta))v(t))dt, \tag{3}$$

where t_i and t_f are the initial and final time, respectively, η_D is the driveline efficiency, and

$$\eta_r = \begin{cases} \eta_R & \text{if } a(t) < 0 \\ 1 & \text{if } a(t) \geq 0 \end{cases} \tag{4}$$

where η_R is the regenerative braking efficiency.

With the reasonable assumption that the road grade is constant, and with $c_1 = m$, $c_2 = \frac{1}{2}\rho CA$, and $c_3 = mg(\mu cos(\theta) + sin(\theta))$, the equation is rewritten as

$$E_w = \frac{1}{\eta_D}\int_{t_i}^{t_f}(\eta_r c_1 a(t)v(t) + c_2 v^3(t) + c_3 v(t))dt. \tag{5}$$

E_w represents the wheel-to-distance energy that is needed to travel between two points, irrespective of the powertrain characteristics. However, the vehicle consumes additional energy to provide auxiliary functions such as air-conditioning, lighting, energy management and a driving control system. Auxiliary consumption varies depending on the travel time. For simplification, we assume that the auxiliary consumption power is constant. Therefore, the energy needed for auxiliary consumption is

$$E_a = \int_{t_i}^{t_f} P_a dt, \tag{6}$$

where E_a is the auxiliary-originated energy consumption and P_a is the instantaneous auxiliary power.

Therefore, the total energy consumption is the summation of the energy needed at wheels and the energy needed for auxiliary consumption. With $c_4 = P_a$, the total energy consumption (E) is

$$E = \frac{1}{\eta_D} \int_{t_i}^{t_f} (\eta_r c_1 a(t) v(t) + c_2 v^3(t) + c_3 v(t) + \eta_D c_4) dt. \quad (7)$$

2.2. Energy Consumption Analytical Parameterization

The definite integral used above cannot be calculated, since $v(t)$ and $a(t)$ have unknown functions and the travel time ($t_f - t_i$) varies according to the vehicle's speed and acceleration. To overcome this issue, we define and analytically parameterize a combination of cruising and accelerating maneuvers. These four scenarios are as follows:

- *Cruise (C):* Cruising with a constant speed over the whole trajectory.
- *Accelerate (A):* Accelerating or decelerating at a constant rate over the whole trajectory.
- *Cruise–accelerate (C-A):* First, cruising at a constant speed over a part of the trajectory; then, accelerating or decelerating with a constant rate over the remainder of the trajectory.
- *Accelerate–cruise (A-C):* First. accelerating or decelerating with a constant rate over a part of the trajectory; then, cruising with a constant speed over the remainder of the trajectory.

We assume that the vehicle's speed profile in free-flow is a part of the speed profile shown in Figure 1. In this regard, part III shows the cruise strategy with $t_1 = t_2 = 0$, part II shows the accelerate strategy with $t_1 = 0$ and $t_2 = t_3$, parts I-and-II shows the cruise–accelerate strategy with $t_2 = t_3$, and parts II-and-III shows the accelerate–cruise strategy with $t_1 = 0$. The main rationale behind this assumption is that the fluctuations in speed cause energy losses because a part of the kinetic energy is lost while braking and recuperation of all the kinetic energy is impossible.

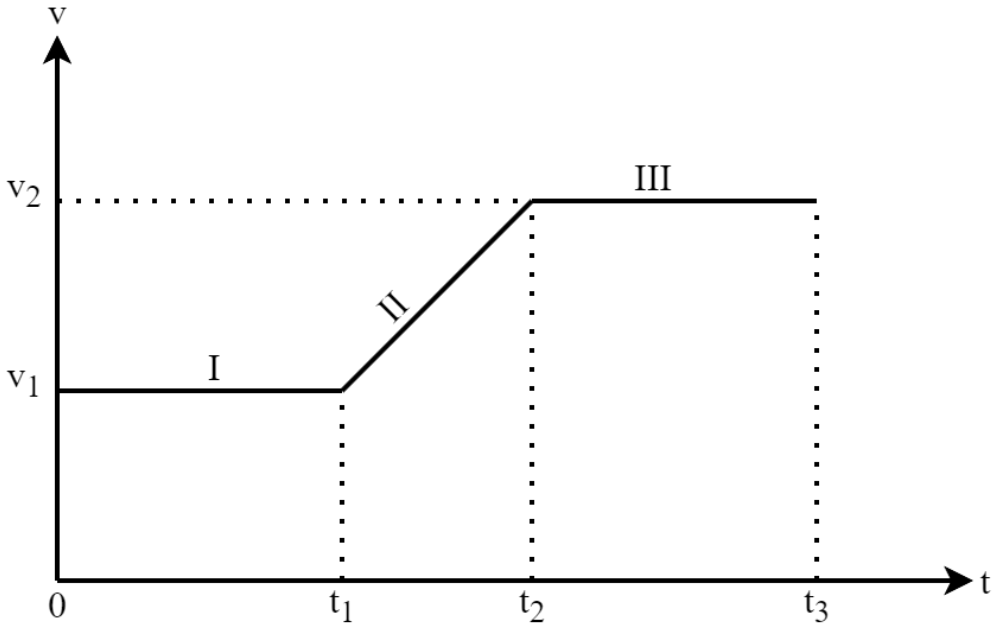

Figure 1. Cruise and accelerate combination strategies.

Based on Figure 1, in $[0, t_1]$ and $[t_2, t]$ (cruising stage), the speed is contant and the acceleration rate is zero. In $[t_1, t_2]$ (accelerating stage), the acceleration rate is constant. The instantaneous speed with a constant acceleration rate is $v(t) = at + v_0$, where v_0 is the initial speed. Therefore, the energy consumption of this scenario during the time interval of $[0, t_3]$ is

$$E = \frac{1}{\eta_D}\int_0^{t_1}(c_2v_1^3 + c_3v_1 + \eta_D c_4)dt + \frac{1}{\eta_D}\int_{t_1}^{t_2}(\eta_r c_1 a(at+v_1) + c_2(at+v_1)^3 + c_3(at+v_1) + \eta_D c_4)dt + \frac{1}{\eta_D}\int_{t_2}^{t_3}(c_2v_2^3 + c_3v_2 + \eta_D c_4)dt. \quad (8)$$

The definite integration in (9) yields

$$E = \frac{1}{\eta_D}[\frac{1}{2}\eta_r m(v_2^2 - v_1^2) + \frac{1}{2}\rho C_a A_f(v_1^3 t_1 + \frac{1}{4a}(v_2^4 - v_1^4) + v_2^3(t_3 - t_2)) + mg(\mu L + \Delta h)] + P_a t_3, \quad (9)$$

where L is the length of the path over which the speed profile is optimized, and Δh is the corresponding elevation difference, which equals zero on flat roads.

Since the time milestones depend on speed and acceleration, we parameterize t_1, t_2, and t_3 in each of the four strategies, based on v_1, v_2, and a. The list of parameterized time milestones is presented in Table 1. For brevity, we present the analytical parameterization process of the cruise-accelerate strategy. The parametization of other strategies can be similarly carried out. During the cruise–accelerate strategy, the traveled distances in part I and part II are

$$\Delta x_I = v_1 t_1, \quad (10)$$

and

$$\Delta x_{II} = \frac{v_2^2 - v_1^2}{2a}. \quad (11)$$

Thus, the whole path length (L) is the summation of the traveled distance in these two parts, which is

$$\Delta x_I + \Delta x_{II} = L. \quad (12)$$

the constant acceleration rate in the accelerating part (part II) is

$$a = \frac{v_2 - v_1}{t_2 - t_1}. \quad (13)$$

Table 1. Analytical parameterization of t_1, t_2, and t_3 for each strategy.

Strategy	t_1	t_2	t_3
C	0	0	$\frac{L}{v_2}$
A	0	$\frac{2L}{v_1+v_2}$	$\frac{2L}{v_1+v_2}$
C-A	$\frac{2aL+v_1^2-v_2^2}{2av_1}$	$\frac{2aL-(v_2-v_1)^2}{2av_1}$	$\frac{2aL-(v_2-v_1)^2}{2av_1}$
A-C	0	$\frac{v_2-v_1}{a}$	$\frac{2aL+(v_2-v_1)^2}{2av_2}$

By substituting Equations (11) and (12) in the Equation (10), t_1 is parameterically calculated as

$$t_1 = \frac{2aL + v_1^2 - v_2^2}{2av_1}. \quad (14)$$

similarly, by substituting Equation (14) in the Equation (13), t_2 will be

$$t_2 = \frac{2aL - (v_2 - v_1)^2}{2av_1}. \quad (15)$$

since $t_2 = t_3$, all the time milestones of the cruise–accelerate strategy are parameterically known.

2.3. Eco-Ff Problem

In each scenario of the eco-FF problem, depending on whether the vehicle is upstream or downstream, the decision variables are v_2 and a, and v_1 and a, respectively. With $v_1 = v_i$ upstream and $v_2 = v_d$ downstream, the energy consumption in the upstream, E_{up}, and downstream, E_{down}, is

$$E_{up} = \frac{1}{\eta_D}[\frac{1}{2}\eta_r m(v_s^2 - v_i^2) + \frac{1}{2}\rho C_a A_f(v_i^3 t_{1u} + \frac{1}{4a_u}(v_s^4 - v_i^4) + v_s^3(t_{3u} - t_{2u})) + mg(\mu L_u + \Delta h_u)]P_a t_{3u}, \tag{16}$$

and

$$E_{down} = \frac{1}{\eta_D}[\frac{1}{2}\eta_r m(v_d^2 - v_s^2) + \frac{1}{2}\rho C_a A_f(v_s^3 t_{1d} + \frac{1}{4a_d}(v_d^4 - v_s^4) + v_d^3(t_{3d} - t_{2d})) + mg(\mu L_d + \Delta h_d)] + P_a t_{3d}. \tag{17}$$

where v_s in the vehicle's speed when it reaches the traffic light stop line, t_{1u}, t_{2u}, and t_{3u} are the parameterized time milestones upstream, t_{1d}, t_{2d}, and t_{3d} are the parameterized time milestones downstream, L_u and L_d are the length of the upstream and downstream path, and Δh_u and Δh_d are the elevation differences between the upstream and downstream paths, respectively.

Consider the vehicle enters the traffic signal's DSRC range, which is L_u distance units from the intersection, and its initial speed is v_i. The shortest time in which the vehicle can reach the intersection is

$$t_s = \frac{2a_{max}L_u + (v_{max} - v_i)^2}{2a_{max}v_{max}}, \tag{18}$$

where a_{max} is the maximum allowed acceleration rate and v_{max} is the maximum speed limit.

Based on the SPAT information, consider p ordered green periods as $\tau_1, \tau_2, \ldots, \tau_p$. Each τ_q for $q \in \{1, 2, \ldots, p\}$ is $\tau_q = [\tau_{q1}, \tau_{q2})$. t_s falls into the Qth interval, τ_Q, if $\tau_{(Q-1)2} \leq t_s \leq \tau_{Q2}$.

Therefore, the eco-FF optimization problem

$$\min_{v_s, a} \; E_{up} + E_{down} \tag{19a}$$

$$s.t. \; v_{min} \leq v_s \leq v_{max} \tag{19b}$$

$$a_{min} \leq a \leq a_{max} \tag{19c}$$

$$\tau_{(Q-1)2} \leq t_{3u} \leq \tau_{Q2}, \tag{19d}$$

where v_{min} is the minimum possible speed that is equal to zero and a_{min} is the maximum allowed deceleration rate. In this problem, Equations (19b) and (19c) correspond to the speed and acceleration limits, and Equation (19d) prevents the red signal violation. The Equation (19a) is a five-degree polynomial optimization problem (w.r.t v_s). According to [29] finding analytical solutions for polynomial problems is extremely difficult compared to finding numerical ones. Additionally, the existence of a green and red timing creates a non-convex problem that further complicates the provision of an analytical solution of Equation (19a). To the best of the authors' knowledge, there is no analytical approach that can solve such a complex problem. However, as the decision variables have three dimenstions, numerical solutions such as global search can be utilized. Therefore, a global search approach is used in this research.

2.4. Human Driver Simulation

As a benchmark, we compare the eco-FF results with the Gipps model and Intelligent Driver Model (IDM) to resemble a human driver.

According to the Gipps model [30], the vehicle's instantaneous speed can be calculated based on (20)–(22).

$$v_e(t+\tau) = min[v_{acc}, v_{dec}] \tag{20}$$

$$v_{acc} = v_e(t) + 2.5a_e\tau(1 - \frac{v_e(t)}{v_{des}(t)})\sqrt{0.025 + \frac{v_e(t)}{v_{des}(t)}} \tag{21}$$

$$v_{dec} = b_e\tau + \sqrt{(b_e\tau)^2 - b_e[2(x_p(t) - x_e(t) - S_p) - v_e(t)\tau - \frac{{v_p}^2(t)}{b_p}]} \tag{22}$$

where $v_e(t)$ is the controlled vehicle's speed at time t, a_e is the maximum acceleration of the controlled vehicle, τ is the reaction time, $v_{des}(t)$ is the desired speed at time t, b_e is the most severe braking of the controlled vehicle (and is negative), $x_p(t)$ is the preceding vehicle's position at time t, $x_e(t)$ is the controlled vehicle's position at time t, S_p is the minimum distance to the preceding vehicle, $v_p(t)$ is the preceding vehicle's speed at time t, and b_p is the most severe estimated braking of the preceding vehicle (and is negative). In this regard, a_e, b_e, b_p, S_p, and τ are parameters that can be calibrated and adapted based on the case, e.g., the weather conditions. The Gipps model is capable of driving simulations either in the presence of a preceding vehicle or in free-flow situations. To make the Gipps model simulate free-flow situations, one can assume that the preceding vehicle is a very far and fast-moving vehicle. In this regard, $x_p \to \infty$, $v_p \to \infty$, $b_p = 0$, and $S_p = 0$.

The second benchmarking baseline is the IDM [31]. According to the IDM, the vehicle's instantaneous acceleration rate can be calculated based on Equations (23) and (24)

$$a_{idm}(t) = a_m[1 - (\frac{v_c(t)}{v_{des}})^\delta - (\frac{s^*(t)}{s_c(t)})^2] \tag{23}$$

$$s^*(t) = s_0 + v_c(t)T + \frac{v_c(t)[v_c(t) - v_1(t)]}{2\sqrt{a_m b_m}} \tag{24}$$

where $a_{idm}(t)$ is the controlled vehicle's acceleration at time t, a_m is the maximum acceleration of the controlled vehicle, $v_c(t)$ is the vehicle's speed at time t, v_{des} is the desired speed, δ is the free acceleration exponent, $s_c(t)$ is the vehicle's location at time t, s_0 is the minimum distance between the controlled vehicle and the preceding vehicle, T is the desired time gap, $v_1(t)$ is the preceding vehicle's speed at time t, and b_m is the absolute value of the vehicle's maximum braking rate. a_m, b_m, s_0, δ, and T are the model parameters: the first four were chosen in accordance with the eco-FF problem and the latter was chosen based on [31].

3. Results

In the first part of this section, we present the calibrated real-world measurements of our work. In these measurements, a BMW i3 vehicle was used, on which several sensors were installed to accurately measure the energy consumption, location, vehicle dynamics, and corresponding time. A detailed description of the vehicle specifications is presented on the manufacturer's website [32]. The majority of the measured data were gathered in Brussels, Belgium. Other values related to environmental parameters were set based on [33]. All the aforementioned parameters and their values are presented in Table 2.

3.1. Measurement

The energy consumption of the vehicle was calibrated based on real-world measured data. During the calibration process, the driveline efficiency and regenerative braking efficiency were calibrated to 92% and 79%, respectively. Based on the environmental temperature and desired cabin temperature, three different levels of auxiliary power consumption were derived: 970 W, 1760 W, and 2550 W for low, medium, and high auxiliary power consumption, respectively.

Table 2. Parameter values of measurements.

Parameter	Value	Parameter	Value
Driveline efficiency: η_D	0.92	Frontal area: A_f	2.38 (m^2)
Regenerative efficiency: η_R	0.79	Vehicle's mass: m	1270 (Kg)
Rotating parts' mass factor: f_m	1.05	Upstream distance: L_u	300 (m)
Friction coefficient: μ	0.01	Downstream distance: L_d	200 (m)
Gravitational acceleration: g	9.81 (m/s^2)	Min. acceleration: a_{min}	-3.5 (m/s^2)
Air density: ρ	1.176 (Kg/m^3)	Max. acceleration: a_{max}	3.5 (m/s^2)
Air drag coefficient: C_a	0.29	Max. speed limit: v_{max}	70 (km/h)

Figure 2 illustrates the theoretical prediction and real-world measured power consumption of the used vehicle. The auxiliary power consumption in this figure is 1760 W, which corresponds to the medium auxiliary power consumption. This shows that the model predicts the power consumption with high accuracy. The Normalized Root Mean Squared Error (NRMSE) is 0.0728, which indicates high model precision.

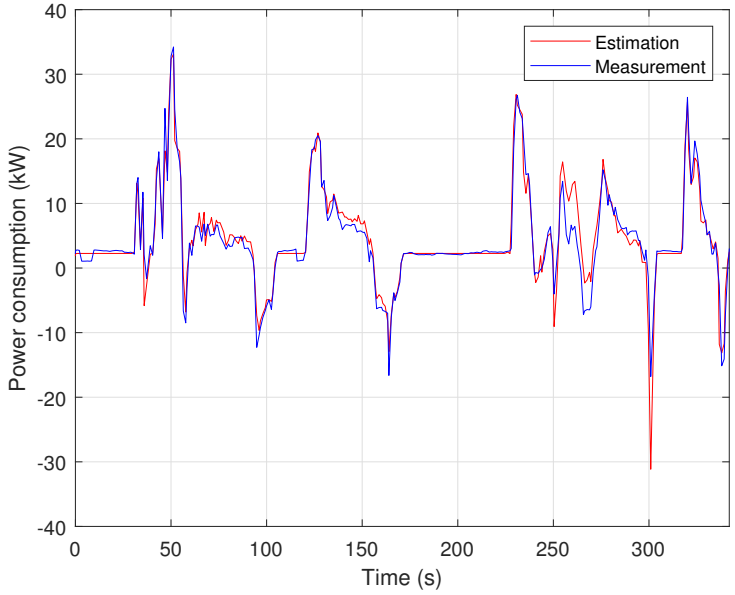

Figure 2. Theoretical prediction and real-world measurement of energy consumption.

3.2. Results and Comparison

By virtue of the power consumption model that was verified in the previous section, in the following, we study the performance of the eco-FF framework. The Gipps model and IDM were utilized as a baseline for the performance benchmark.

Figure 3 represents the optimal speed profiles of eco-FF, Gipps, and IDM models in four different settings, in which the initial and desired speeds provide realistic values at the interval of $[0 \quad 70]$ km/h, in accordance with the general urban speed limits.The auxiliary power consumption (c_4) was selected as 970 W and 2550 W to represent low and high consumption levels, respectively, based on the real-world data measurements. For the Gipps model, τ was assumed to be 0.5 s, a_e as a_{max}, b_e and b_p to be a_{min}, v_{des} to be v_d, and S_p to be zero. For the IDM, T was assumed to be 0.5 s, a_m to be a_{max}, b_m to be $|a_{min}|$, v_{des} to be v_d, s_0 to be zero, and δ to be 4. Additionally, the corresponding green and red light periods for each plot are shown by their color at the bottom of the figures. Figure 3a shows that the eco-FF method chose the $A-C$ and A strategies in up- and downstream, respectively. In the $A-C$ strategy, the speed profile was chosen to catch the beginning of the second green period while avoiding sudden speed changes. However, the Gipps model and IDM led to an overshoot of speed and reached the intersection during the red period, which increased the energy consumption and reduced the comfort level. The difference in energy

consumption between the eco-FF and Gipps models was 0.0531 kWh, which is equal to 28.49% energy savings. The difference in energy consumption between the eco-FF and IDM was 0.0304 kWh, which is equal to 18.58% energy savings. The strategy chosen in Figure 3b by the eco-FF model was A and A for both up- and downstream. The same energy-saving behavior was observed in the speed profile of the eco-FF method, whereas the Gipps model and IDM underwent an unnecessary acceleration and deceleration, resulting in a higher energy consumption. The difference in energy consumption between the eco-FF and Gipps models was 0.0562 kWh, which is equal to 33.86% energy savings. The energy consumption difference between the eco-FF and IDM was 0.0161 kWh, which is equal to 12.77% energy savings. Figure 3c,d were plotted for two different values of c_4 to indicate the importance of auxiliary power consumption in the speed profile of the considered methods. We can see that, regardless of c_4, the Gipps model and IDM had almost identical behaviors in both cases. In contrast, the eco-FF method actively adjusts its speed to take advantage of the imposed conditions. When the auxiliary power consumption is low, the eco-FF model prefers reducing the acceleration and increasing the travel time (almost 45 s). In this case, power consumption was dominated by the changes in speed. However, for higher values of c_4 the eco-FF method chose to utilize increased accelerations and reach the desired speed and location in a shorter time (36.5 s) because the total energy consumption was dominated by the auxiliary energy consumption. The difference in energy consumption between the eco-FF and Gipps models was 0.0141 kWh and 0.0109 kWh, which is equal to 15.25% and 9.56% energy savings, respectively. The energy consumption difference between the eco-FF model and IDM was 0.0184 kWh and 0.0149 kWh, which is equal to 19.05% and 12.66% energy savings, respectively.

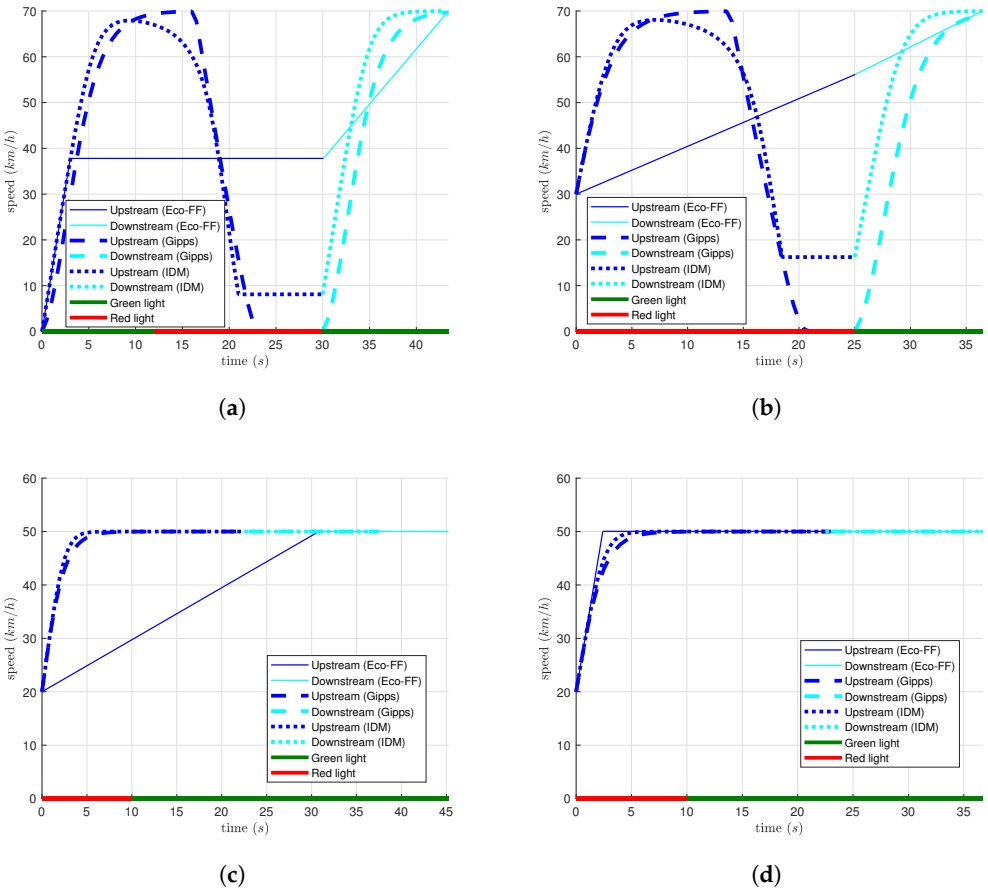

Figure 3. The eco-FF, Gipps, and IDM models' speed behaviors. (**a**) $v_i = 0$ (km/h), $v_d = 70$ (km/h), and $c_4 = 970$ (W). (**b**) $v_i = 30$ (km/h), $v_d = 70$ (km/h), and $c_4 = 970$ (W). (**c**) $v_i = 20$ (km/h), $v_d = 50$ (km/h), and $c_4 = 970$ (W). (**d**) $v_i = 20$ (km/h), $v_d = 50$ (km/h), and $c_4 = 2550$ (W).

In Figure 4, the blue boxes show the interquartile range, which contains the most probable energy-saving values, and the gray planes show the min/max values. In Figure 4a, which represents a low level of auxiliary power consumption, there is a high performance difference between the eco-FF and Gipps model, especially for higher values of both v_i and v_d. As c_4 increases, the difference between these two models decreases, as shown in Figure 4b. This behavior is also observed in Figure 3c,d, where the speed profile of both models became more similar when the auxiliary power consumption was increased.

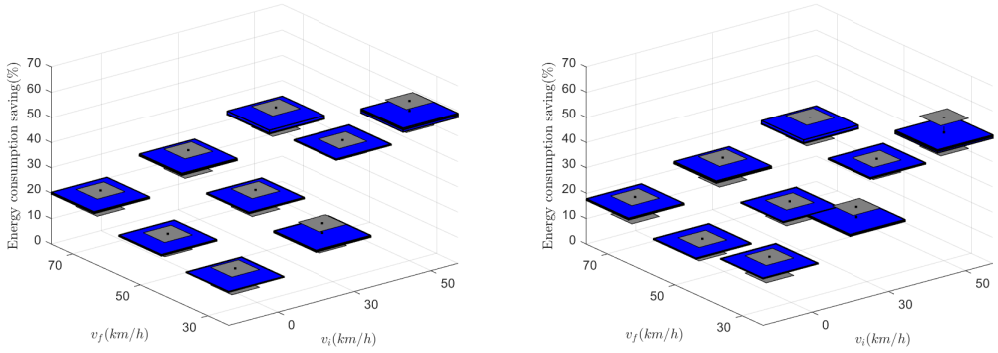

(**a**) (**b**)

Figure 4. Energy consumption savings of the eco-FF model with respect to the Gipps model with low and high auxiliary power consumption levels. (**a**) $c_4 = 970$ (W). (**b**) $c_4 = 2550$ (W).

Figure 4 illustrates the energy consumption savings of the eco-FF model in comparison to the Gipps model. The x-axis and the y-axis represent the v_i and v_d, respectively. For each pair of (v_i, v_d), 100 randomly generated realizations of SPaT are simulated. In every realization, the SPaT is 15 s and 35 s for red and green intervals, respectively, which sums up to a 50 s periodic timeline. During the green timespan of each 50 s timeline, there is a 50% probability of a one-time actuation caused by crossing vehicles or pedestrians. If actuation is requested, a 5 s red light will occur during the 35 s green light. Additionally, to determine the beginning phase of the traffic signal (green or red), the phase was randomly chosen based on a uniform distribution between 0 and 50. Figure 5 shows 25 realization examples of SPaT.

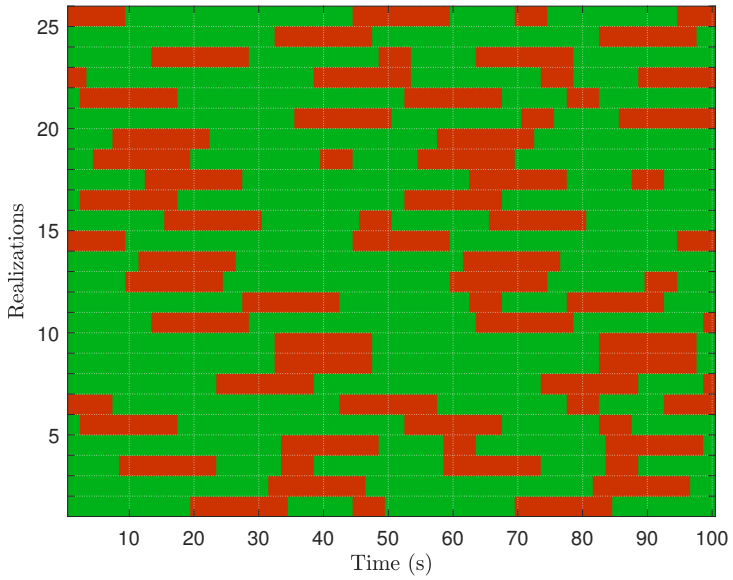

Figure 5. Signal green and red intervals for 25 realizations.

Figure 6 illustrates the travel time difference between the eco-FF model and the Gipps model. The x- and y-axes are the same as in the previous plot. The boxes show the percentage of travel time reductions in the eco-FF model in comparison to the Gipps model. The blue boxes represent the realizations in which the eco-FF model travel time was shorter than the Gipps model. The red boxes show the increase in eco-FF model travel time in comparison to the Gipps model. Comparing the Figure 6a,b, which represent the low and high levels of c_4, respectively, one can see that, by increasing c_4, the behavior of the eco-FF model tends to choose higher levels of speed. At high levels of c_4, the time-dependent auxiliary consumption is dominant. Additionally, both plots illustrate that, at lower desired final speeds, the eco-FF model outperforms in terms of travel time. This is because the Gipps model tends to reach the desired speed as soon as possible and then cruise at that speed, while the eco-FF model speed is optimally determined based on the SPaT, c_4, and the initial and desired final speeds.

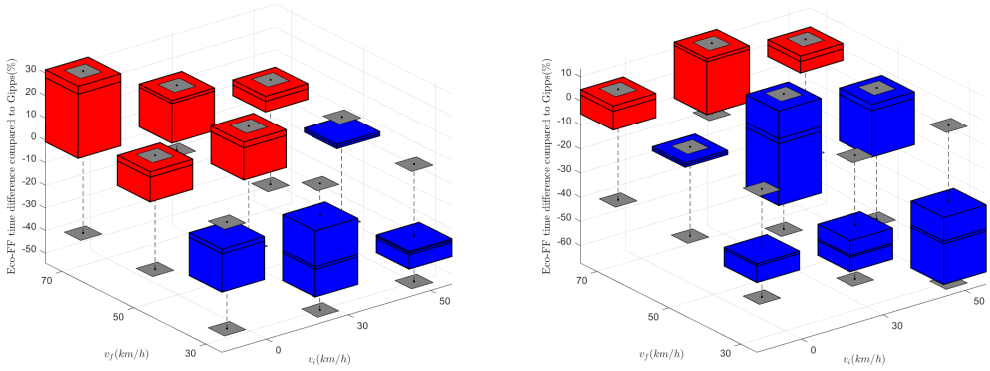

(**a**) (**b**)

Figure 6. Eco-FF travel time difference compared to the Gipps with low and high auxiliary power consumption levels. (**a**) $c_4 = 970$ (W). (**b**) $c_4 = 2550$ (W).

4. Conclusions

The research work in this paper developed an eco-FF framework to optimize AV energy consumption levels when approaching and departing from a signalized intersection. The eco-FF framework jointly optimized the AV's behavior both up- and downstream. In addition, by adding the time-dependent auxiliary power consumption, the travel time was incorporated into the cost function. The framework used the SPaT information collected via V2I communication to calculate the optimal AV speed profile. The problem was analytically parameterized under the assumption that the road grade is constant. These simulations showed that the energy consumption savings were greater at lower auxiliary power consumption levels. This reduction in energy consumption reached 63.09% and 56.66% at low and high levels of auxiliary power consumption, respectively. In addition, the eco-FF model travel time saving reached 54.52% and 67.27% at low and high levels of auxiliary power consumption, respectively. Therefore, the simulation results reveal the strong influence of auxiliary power consumption on the optimal speed profile. To calibrate the model parameters and verify the precision of the presented energy consumption model, real-world measurements were used, focusing on the energy consumption, location and speed profile of a BMW i3 in the city of Brussels, Belgium.

At present, the proposed framework is exclusively applicable to free-flow traffic. In the future, we plan to use the presented eco-FF framework as the higher level of a comprehensive eco-driving logic in the presence of other road users. We could integrate the eco-driving by using cooperative adaptive cruise control as the lower layer of the comprehensive framework. Moreover, we will use the optimization-based control algorithms for real-time use. Additionally, the auxiliary consumption term can be modified for use in different vehicle operation modes at different levels of auxiliary power consumption.

Author Contributions: Conceptualization, S.H. and C.D.C.; methodology, S.H. and C.D.C.; software, S.H.; validation, S.H. and C.D.C.; formal analysis, C.D.C., E.R. and L.V.; investigation, S.H., C.D.C. and E.R.; resources, C.D.C., L.V. and T.C.; data curation, C.D.C. and T.C.; writing—original draft preparation, S.H.; writing—review and editing, S.H., C.D.C., E.R. and L.V.; visualization, S.H. and C.D.C.; supervision, C.D.C., E.R., L.V. and T.C.; project administration, L.V. and T.C.; funding acquisition, T.C. All authors have read and agreed to the published version of the manuscript.

Funding: This research was funded by SRP56: SRP-Onderzoekszwaartepunt: Autonomous Mobility & Logistics.

Institutional Review Board Statement: Not applicable.

Informed Consent Statement: Not applicable.

Data Availability Statement: Not applicable.

Conflicts of Interest: The authors declare no conflict of interest.

References

1. Hao, P.; Wu, G.; Boriboonsomsin, K.; Barth, M.J. Eco-approach and departure (EAD) application for actuated signals in real-world traffic. *IEEE Trans. Intell. Transp. Syst.* **2018**, *20*, 30–40. [CrossRef]
2. De Nunzio, G.; Gomes, G.; Canudas-de Wit, C.; Horowitz, R.; Moulin, P. Speed advisory and signal offsets control for arterial bandwidth maximization and energy consumption reduction. *IEEE Trans. Control. Syst. Technol.* **2016**, *25*, 875–887. [CrossRef]
3. Xia, H.; Boriboonsomsin, K.; Schweizer, F.; Winckler, A.; Zhou, K.; Zhang, W.B.; Barth, M. Field operational testing of eco-approach technology at a fixed-time signalized intersection. In Proceedings of the 2012 15th International IEEE Conference on Intelligent Transportation Systems, Pittsburgh, PA, USA, 15–18 July 2012; pp. 188–193.
4. Yang, H.; Almutairi, F.; Rakha, H. Eco-driving at signalized intersections: A multiple signal optimization approach. *IEEE Trans. Intell. Transp. Syst.* **2020**, *22*, 2943–2955. [CrossRef]
5. Ma, F.; Yang, Y.; Wang, J.; Li, X.; Wu, G.; Zhao, Y.; Wu, L.; Aksun-Guvenc, B.; Guvenc, L. Eco-driving-based cooperative adaptive cruise control of connected vehicles platoon at signalized intersections. *Transp. Res. Part Transp. Environ.* **2021**, *92*, 102746. [CrossRef]
6. Gilbert, E.G. Vehicle cruise: Improved fuel economy by periodic control. *Automatica* **1976**, *12*, 159–166. [CrossRef]
7. Hooker, J.N. Optimal driving for single-vehicle fuel economy. *Transp. Res. Part A Gen.* **1988**, *22*, 183–201. [CrossRef]
8. Hellström, E.; Åslund, J.; Nielsen, L. Design of an efficient algorithm for fuel-optimal look-ahead control. *Control Eng. Pract.* **2010**, *18*, 1318–1327. [CrossRef]
9. Rakha, H.; Kamalanathsharma, R.K. Eco-driving at signalized intersections using V2I communication. In Proceedings of the 2011 14th International IEEE Conference on Intelligent Transportation Systems (ITSC), Washington, DC, USA, 5–7 October 2011; pp. 341–346.
10. Ala, M.V.; Yang, H.; Rakha, H. Modeling evaluation of eco–cooperative adaptive cruise control in vicinity of signalized intersections. *Transp. Res. Rec.* **2016**, *2559*, 108–119. [CrossRef]
11. Jiang, H.; Hu, J.; An, S.; Wang, M.; Park, B.B. Eco approaching at an isolated signalized intersection under partially connected and automated vehicles environment. *Transp. Res. Part Emerg. Technol.* **2017**, *79*, 290–307. [CrossRef]
12. Yang, H.; Rakha, H.; Ala, M.V. Eco-cooperative adaptive cruise control at signalized intersections considering queue effects. *IEEE Trans. Intell. Transp. Syst.* **2016**, *18*, 1575–1585. [CrossRef]
13. Mandava, S.; Boriboonsomsin, K.; Barth, M. Arterial velocity planning based on traffic signal information under light traffic conditions. In Proceedings of the 2009 12th International IEEE Conference on Intelligent Transportation Systems, St. Louis, MO, USA, 4–7 October 2009; pp. 1–6.
14. Barth, M.; Mandava, S.; Boriboonsomsin, K.; Xia, H. Dynamic ECO-driving for arterial corridors. In Proceedings of the 2011 IEEE Forum on Integrated and Sustainable Transportation Systems, Vienna, Austria, 29 June–1 July 2011; pp. 182–188.
15. HomChaudhuri, B.; Vahidi, A.; Pisu, P. A fuel economic model predictive control strategy for a group of connected vehicles in urban roads. In Proceedings of the 2015 American Control Conference (ACC), Chicago, IL, USA, 1–3 July 2015; pp. 2741–2746.
16. Wang, Z.; Wu, G.; Hao, P.; Boriboonsomsin, K.; Barth, M. Developing a platoon-wide eco-cooperative adaptive cruise control (CACC) system. In Proceedings of the 2017 Ieee Intelligent Vehicles Symposium (iv), Los Angeles, CA, USA, 11–14 June 2017; pp. 1256–1261.
17. Asadi, B.; Vahidi, A. Predictive cruise control: Utilizing upcoming traffic signal information for improving fuel economy and reducing trip time. *IEEE Trans. Control. Syst. Technol.* **2010**, *19*, 707–714. [CrossRef]
18. Mahler, G.; Vahidi, A. Reducing idling at red lights based on probabilistic prediction of traffic signal timings. In Proceedings of the 2012 American Control Conference (ACC), Montreal, QC, Canada, 27–29 June 2012; pp. 6557–6562.
19. Mahler, G.; Vahidi, A. An optimal velocity-planning scheme for vehicle energy efficiency through probabilistic prediction of traffic-signal timing. *IEEE Trans. Intell. Transp. Syst.* **2014**, *15*, 2516–2523. [CrossRef]

20. Chen, P.; Yan, C.; Sun, J.; Wang, Y.; Chen, S.; Li, K. Dynamic eco-driving speed guidance at signalized intersections: Multivehicle driving simulator based experimental study. *J. Adv. Transp.* **2018**, *2018*, 6031764. [CrossRef]
21. Oh, G.; Peng, H. Eco-driving at signalized intersections: What is possible in the real-world? In Proceedings of the 2018 21st International Conference on Intelligent Transportation Systems (ITSC), Maui, HI, USA, 4–7 November 2018; pp. 3674–3679.
22. Sun, C.; Guanetti, J.; Borrelli, F.; Moura, S.J. Optimal eco-driving control of connected and autonomous vehicles through signalized intersections. *IEEE Internet Things J.* **2020**, *7*, 3759–3773. [CrossRef]
23. Kamalanathsharma, R.K.; Rakha, H.A. Multi-stage dynamic programming algorithm for eco-speed control at traffic signalized intersections. In Proceedings of the 16th International IEEE Conference on Intelligent Transportation Systems (ITSC 2013), The Hague, The Netherlands, 6–9 October 2013; pp. 2094–2099.
24. Mousa, S.R.; Ishak, S.; Mousa, R.M.; Codjoe, J. Developing an eco-driving application for semi-actuated signalized intersections and modeling the market penetration rates of eco-driving. *Transp. Res. Rec.* **2019**, *2673*, 466–477. [CrossRef]
25. Tang, T.Q.; Yi, Z.Y.; Zhang, J.; Wang, T.; Leng, J.Q. A speed guidance strategy for multiple signalized intersections based on car-following model. *Phys. A Stat. Mech. Its Appl.* **2018**, *496*, 399–409. [CrossRef]
26. Han, J.; Vahidi, A.; Sciarretta, A. Fundamentals of energy efficient driving for combustion engine and electric vehicles: An optimal control perspective. *Automatica* **2019**, *103*, 558–572. [CrossRef]
27. De Nunzio, G.; De Wit, C.C.; Moulin, P.; Di Domenico, D. Eco-driving in urban traffic networks using traffic signals information. *Int. J. Robust Nonlinear Control* **2016**, *26*, 1307–1324. [CrossRef]
28. Zhang, J.; Tang, T.Q.; Yan, Y.; Qu, X. Eco-driving control for connected and automated electric vehicles at signalized intersections with wireless charging. *Appl. Energy* **2021**, *282*, 116215. [CrossRef]
29. Boyd, S.; Boyd, S.P.; Vandenberghe, L. *Convex Optimization*; Cambridge University Press: Cambridge, UK, 2004.
30. Gipps, P.G. A behavioural car-following model for computer simulation. *Transp. Res. Part B Methodol.* **1981**, *15*, 105–111. [CrossRef]
31. Kesting, A.; Treiber, M.; Helbing, D. Enhanced intelligent driver model to access the impact of driving strategies on traffic capacity. *Philos. Trans. R. Soc. Math. Phys. Eng. Sci.* **2010**, *368*, 4585–4605. [CrossRef] [PubMed]
32. Available online: https://www.press.bmwgroup.com/global/article/attachment/T0284828EN/415571 (accessed on 18 December 2022).
33. Asamer, J.; Graser, A.; Heilmann, B.; Ruthmair, M. Sensitivity analysis for energy demand estimation of electric vehicles. *Transp. Res. Part D Transp. Environ.* **2016**, *46*, 182–199. [CrossRef]